Bioinspired Gradient Poly(ionic liquid) Ionogels for Ionic Skins with an Ultrawide Pressure Detection Range

Xiaoyu Zhang, Sheng Zeng, Zhenyu Hu, Xing Liang, Qi Sun, Jia Huang*, and Guoqing Zu*

Interdisciplinary Materials Research Center, Department of Polymeric Materials, School of Materials Science and Engineering, Tongji University, Shanghai 201804, P.R. China

*Email: huangjia@tongji.edu.cn; guoqingzu@tongji.edu.cn

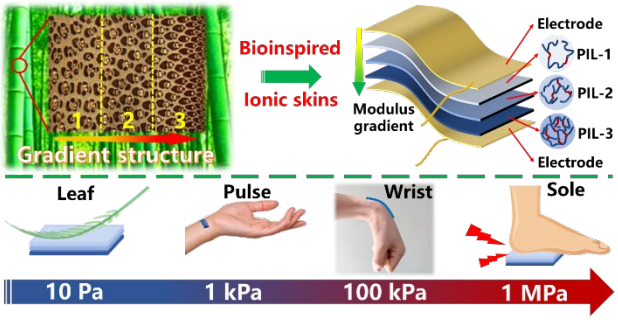

Recently, with the increasing demand for artificial skins and human bodily motion/physical signals monitoring, flexible pressure sensors with a wide detection range are urgently needed. Transparent and stretchable gels with ionic conductivities are considered to be ideal candidates for flexible pressure sensors. However, the gel-based pressure sensors usually show a relatively narrow detection range, which significantly limits their practical applications. Herein, we report an unprecedented bioinspired highly flexible modulus/conductivity-dual-gradient poly(ionic liquid) (PIL) ionogel, which is achieved by constructing three layers of PIL ionogels with different monomer concentrations via a layer-by-layer gelation method. The flexible pressure sensor based on the gradient PIL ionogel exhibits an ultrabroad detection range of 10 Pa-1 MPa. This wearable pressure sensor is highly stable in environments and able to monitor both the tiny pressures as low as 10-100 Pa and the high pressures up to 0.1-1 MPa during human body movements. This work provides a powerful strategy for the preparation of flexible gradient materials that are promising for wearable electronics with a wide pressure detection range.

Stretchable and flexible electronic devices, as new types of intelligent devices, have achieved tremendous growth owing to their portability, flexibility, and real-time feedback. Modern flexible wearable devices are able to monitor, transmit, and analyze human physiological signals and activity status in real time, which show great advantages over conventional devices with the characteristics of rigidness and brittleness.[1, 2] Recently, as a kind of flexible devices, flexible pressure sensors have attracted much attention. The flexible pressure sensors are able to convert the external pressures into quantifiable electrical signals or other signals for transmission, and show potential applications in varied fields such as artificial skins, soft robotics, bioelectronic interfaces, health diagnoses, human bodily motion monitoring, and energy equipment.[3-8] Among the reported pressure-sensitive materials, gels are considered to be ideal candidates because of their ionic conductivity, biocompatibility, high stretchability, and optical transparency.[3, 4, 9] Various flexible pressure sensors based on different kinds of gels such as ionic conductive hydrogels,[9-12] organohydrogels,[13-15] organogels,[16, 17] and ionogels (also called ionic liquid gels) [18, 19] have been reported.

Recently, with the increasing demand for electronic skins and human bodily motion/physical signals monitoring, flexible pressure sensors with a wide detection range are urgently needed.[19-21] The pressure may be as low as 1-10 Pa induced by a lightweight object such as a small leaf put on the skin. Whereas the pressures on the surfaces of human's sole, finger, and palm may reach 100 kPa-1 MPa during some sports such as running, jumping, or grabbing heavy objects by hand.[20, 21] The wearable pressure sensors with the ability to detect both tiny pressures (such as 10-100 Pa) and high pressures (such as 100 kPa-1 MPa) are needed for practical applications.

However, the reported gel-based pressure sensors usually show a relatively narrow pressure detection range, which hardly meet the needs of wide-range pressure sensing in practical applications. The reported flexible pressure sensors based on ionic conductive polyvinyl alcohol (PVA)/polyacrylamide (PAM) hydrogels and cellulose nanofiber/PVA organohydrogels

showed a detection range of 0-35 kPa.[10, 22] The flexible pressure sensors based on amylopectin/poly(acrylic acid-co-acrylamide) organohydrogels possessed a detection range of 10 Pa-65 kPa.[13] The reported poly(vinylidene fluoride-hexafluoropropylene) ionic gel-based pressure sensor with soft micropillared electrodes showed a detection range of 0.9 Pa-176 kPa.[23] The pressure sensors based on ionic conductive chitosan−poly(acrylamide-co-acrylic acid) double-network hydrogel could detect the pressures lower than 260 kPa.[24] The flexible pressure sensor based on chitosan/PAM/polyaniline hydrogel with a high modulus and a high compressive strength was able to detect high pressures up to several megapascals, but its pressure detection limit was relatively high (100 Pa).[9]

The gradient structure of human skins endows them with the ability of sensing wide-range pressures from approximately 1 kPa to 1 MPa.[2, 7, 19] The detection range of the pressure sensors can be effectively enhanced by preparing pressure-sensitive materials with a bioinspired gradient structure.[19, 25, 26] The conductivity-gradient multi-layer flexible pressure sensor based on stiffness-gradient interlocked microdomes and coplanar electrodes showed a broad detection range (0.025 Pa-100 kPa) with high sensitivity and linearity.[25] But it was not able to detect the pressures higher than 100 kPa. Song et al. reported a porous material with a gradient and hierarchical architecture, which endowed the resulted pressure sensor with a wide detection range of 0.4 Pa-400 kPa.[26] Yan et al prepared an ionic liquid gel with a gradient structure induced by an electric field, and the resultant pressure sensor showed a high sensitivity of 1.62 nF kPa^{-1} and a wide detection range of 300 Pa to 2.5 MPa.[19] In spite of the enhanced upper detection limit, its lowest detection pressure was relatively high, and it was not able to detect the tiny pressures lower than 300 Pa. It remains a challenge to achieve ionogel-based pressure sensors with a wider detection range.

Besides, many previously reported water-containing gels were unstable in environments because of the evaporation of water and might be frozen at low temperatures, resulting in the deterioration of device performances.[9-12, 27, 28] Among the ionic conductive gels, ionogels have drawn great attention because of high stability in environments and excellent freeze resistance.[18, 19, 29, 30] Ionic liquids are a class of organic salts composed solely of ions and some of them are in liquid state at room temperature. They have a series of unique properties, such as high ionic conductivity, nonflammability, nonvolatility, and excellent chemical and thermal stabilities, which endow the ionogels with ionic conductivity and high stability in environments.[31, 32] Polymerization of some ionic liquids that containing polymerizable groups such as vinyl groups can afford a new type of ionic conductive gels—poly(ionic liquid) (PIL) gels. The PIL gels possess tunable ionic conductivity and high flexibility and can be applied as electrolytes for high-performance supercapacitors and batteries.[33-35] The solid-state supercapacitor based on a poly(propylsulfonate dimethylammonium propylmethacrylamide) gel electrolyte exhibited superior electrochemical performances with a high volume specific capacitance of 300.8 F cm^{-3} at 0.8 A cm^{-3}.[33] The PIL gels also show potential applications in wearable electronics and electronic skins.[29, 36] Liu et al demonstrated an anti-freezing and highly sensitive ionic skin based on a zwitterionic PIL, featuring high stretchability (900%), and high conductivity (1.1 S m^{-1}) at a low temperature (-20 ℃).[36] The multimodal ionic skin could detect pressures in the range of 1.1 to 45 kPa in the capacitive mode.

Herein, we report a novel bioinspired transparent multi-layer PIL ionogel with a unique modulus/conductivity-dual-gradient porous structure, which significantly enhanced the detection range of the flexible pressure sensor based on the ionogel. The PIL ionogel was prepared by the radical polymerization of an ionic liquid monomer — 1-vinyl-3-butylimidazolium tetrafluoroborate ([VBIm][BF_4]), with N,N'-methylene bisacrylamide (MBA) as the cross-linker and 2-hydroxy-4′-(2-hydroxyethoxy)-2-methylpropiopheno (Irgacure-2959) as the initiator. Another kind of ionic liquid (1-butyl-3-methylimidazolium tetrafluoroborate ([BMIm][BF_4])) was used as the solvent. The modulus/conductivity-dual-gradient structure of the PIL ionogel was achieved by constructing three layers of PIL ionogels with different monomer concentrations via a layer-by-layer gelation method, which was simple and energy efficient. The flexible pressure sensor based on the gradient PIL ionogel exhibited an ultrabroad detection range of 10 Pa-1 MPa. This pressure sensor was wearable and able to monitor both the tiny pressures (10-100 Pa) and the high pressures (0.1-1 MPa) of various physiological signals and human bodily motions. This work provides a powerful strategy towards flexible gradient materials promising for wearable electronics with a wide pressure detection range.

As shown in **Figure 1a**, bamboo culms are a kind of structurally gradient materials, which possess gradient distributions of longitudinal fibers through the wall thickness. The concentration of longitudinal fibers gradually increases from inside to outside, making bamboo a high-strength material.[37] Inspired by the gradient structure of bamboo culms, the multi-layer gradient PIL ionogel was prepared by a layer-by-layer gelation method as shown in **Figure 1b** and **Figure S1**. Radical polymerization of the ionic liquid monomer [VBIm][BF_4] at the presence of the cross linker MBA, the photoinitiator Irgacure-2959, and the solvent [BMIm][BF_4] could afford an ionogel with a three-dimensional (3D) cross-linked PIL network structure (**Figure 1c**). The porous structure, mechanical property, and electrical conductivity of the PIL ionogel could be adjusted by changing the concentrations of the monomer in the mixed solution during the preparation of different ionogel layers. The pressure/strain sensor based on the multi-layer gradient PIL ionogel is expected to possess a wide pressure detection range.

The cylindrical and rectangular gradient PIL ionogels could be obtained simply by layer-by-layer gelation in a beaker and a rectangular container, respectively. The gradient PIL ionogel had high optical transparency, which is necessary for transparent electronics (**Figure 2a**). The three ionogel layers were firmly bonded to each other without separation during processing, compression, and stretching.

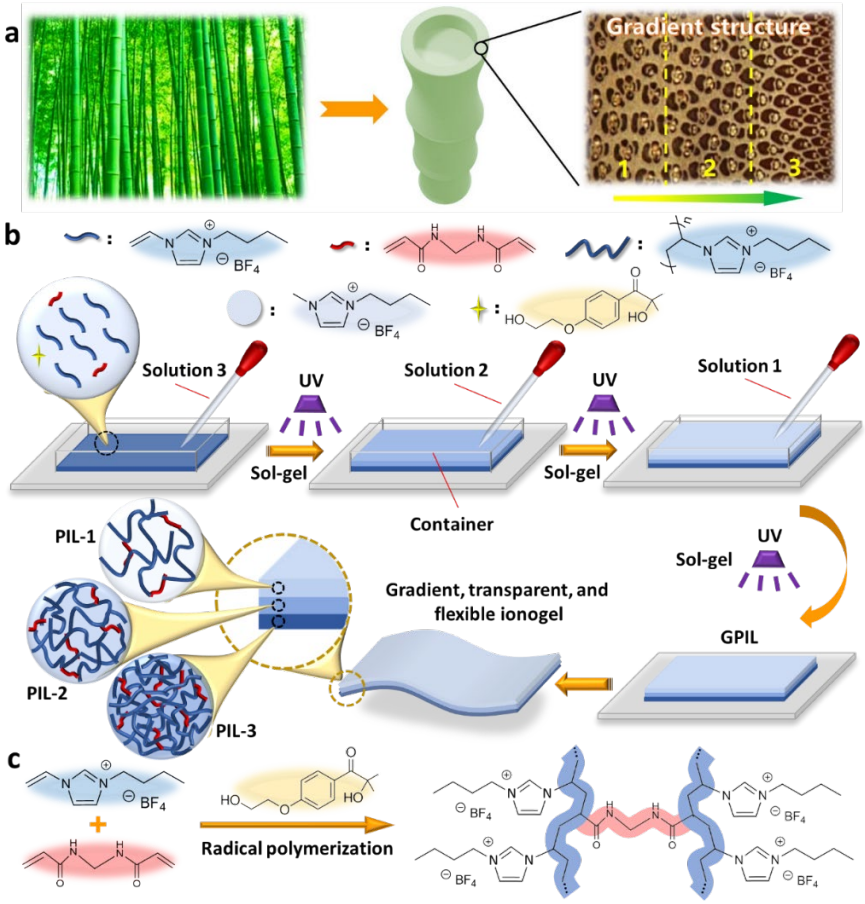

Figure 1. Mechanism and preparation method of the multi-layer gradient PIL ionogels. (a) Overview of the cross section of the bamboo culms with gradient distributions of longitudinal fibers: Reproduced with permission: Copyright 2006, Springer.[37] (b) Illustration showing the preparation process of the gradient PIL ionogel via a layer-by-layer gelation method. (c) Schematic of the network formation via the radical polymerization method.

The concentration variation of the monomer during preparation could be used to adjust the porous structures of the resulting PIL ionogels. The cross-linked network structure of the PIL ionogels was achieved by polymerization of the monomer at the presence of a cross linker. The monomer concentration during preparation could affect the cross-linking density of the resulted polymer network. The higher monomer concentration resulted in higher cross-linking density, while the lower monomer concentration resulted in lower cross-linking density. The higher cross-linking density of the polymer network could lead to the smaller pore size, whereas the lower cross-linking density could lead to the larger pore size.

Field emission scanning electron microscopy (FESEM) was used to observe the microstructures of PIL ionogels. Note that the ionic liquid [BMIm][BF_4] was freeze-resistant and not volatile. Therefore, the ionic liquids in the PIL ionogels were replaced with water to afford hydrogels, which were then freeze-dried to remove water before the FESEM test. The pore size of PIL-3 was significantly smaller than those of PIL-1 and PIL-2, and the pore walls became thicker with increasing the monomer concentration (**Figure 2b**). The FESEM images of PIL-1, PIL-2, and PIL-3 indicated the gradient porous structure of GPIL. The PIL ionogel with thicker pore walls was expected to have a tougher skeleton with higher Young's modulus and compressive strength, which was confirmed by the mechanical tests described below.

The chemical structure of PIL-1 was investigated by FTIR (**Figure 2c**). The bands at 3342 cm^{-1} and 3153 cm^{-1} were ascribed to the C-H stretching vibration of imidazole ring, while the bands at 2964 cm^{-1}, 2920 cm^{-1} and 2878 cm^{-1} were attributed to the stretching vibration of aliphatic C-H.[38] The band at 1573 cm^{-1} corresponded to the stretching vibration of C=C on imidazole ring skeleton,[39] while those at 1467 cm^{-1} and 1165 cm^{-1} were ascribed to the deformation vibration of -CH_3 on imidazole ring and the in-plane deformation vibration of imidazole ring C-H, respectively.[40] The band at 1083 cm^{-1} corresponded to the stretching vibration of B-F in BF_4.

Traditional hydrogels are unstable in environments because of the evaporation of water and the freeze at low temperatures, which significantly limit their applications as flexible pressure sensors. However, the ionic liquids used in this work were characterized by their nonvolatility, chemical stability, and wide working temperature range, which endowed the resulting GPIL with excellent anti-freezing performances and high stability in environments. When placing GPIL in a refrigerator at -17 °C for 24 h, it still maintained high flexibility and stretchability, which showed excellent freeze resistance of GPIL (**Figure 2d**). The appearance, weight, volume, and shape of GPIL remained nearly unchanged after being placed in indoor air for 3 months (**Figure 2e**), indicating the high environmental stability. In addition, GPIL exhibited excellent self-adhesive and self-healing properties (**Figure 2f** and **Figure S2**). After being cut into two pieces, they can be bonded to each

other in 5 seconds under ambient conditions and the recombined GPIL can be stretched with approximately 100% strain without fracture (**Movie S1**). The imidazolium cation of the monomer ([VBIm][BF_4]) and solvent ([BMIm][BF_4]) could form strong interactions with BF_4^- via ionic bond.[29] The reconstruction of ionic bond may lead to the self-healing behavior of the PIL ionogels.

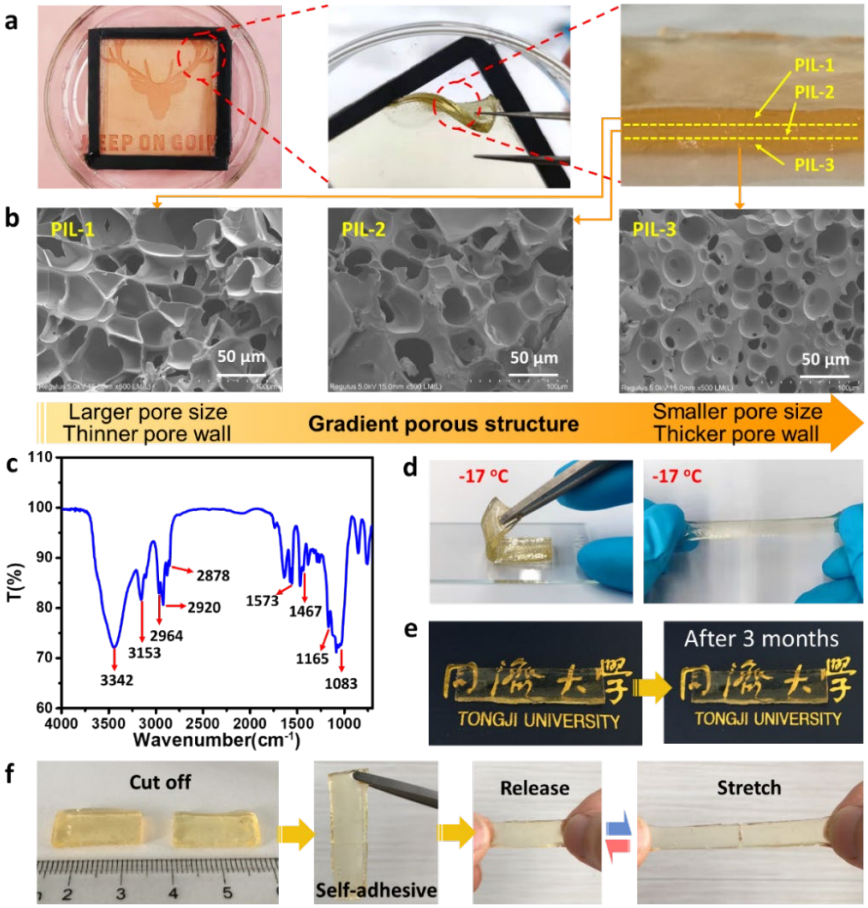

Figure 2. Appearances, morphologies, chemical structures, environmental stability, and self-adhesion of the multi-layer gradient PIL ionogel. (a) Digital photos of GPIL. (b) FESEM images of PIL-1, PIL-2, and PIL-3 showing a gradient porous structure of GPIL. (c) FTIR spectrum of PIL-1. (d) The flexibility and stretchability of GPIL after being placed in a refrigerator at -17 °C for 24 h. (e) Environmental stability of GPIL in air for 3 months. (f) Self-adhesive properties of GPIL.

The compressive stress-strain curves of PIL-1, PIL-2, PIL-3, and GPIL were shown in **Figure 3a-f**, **Figure S3**, **Figure S4**, and **Figure S5**. GPIL and each layer of GPIL were able to withstand 80% compression without fracture and recover their initial states after they were released, demonstrating their high compressibility and elasticity. By comparing the compressive stress-strain curves of the PIL ionogels, we found that the compressive strengths and moduli of the PIL ionogels could be adjusted in a wide range by changing the concentrations of the ionic liquid monomer [VBIm][BF_4].

The compressive strengths and Young's moduli of the PIL ionogels became higher with the increase of monomer concentrations. The compressive stresses of PIL-1 and PIL-2 at 80% strain were around 120 kPa and 251 kPa, respectively, while those of PIL-3 and GPIL reached 1200 kPa and 809 kPa, respectively (**Figure 3a-d**). In addition, the Young's modulus increased from 4 kPa for PIL-1 to 25 kPa for PIL-2 and then 144 kPa for PIL-3 (**Figure 3i**). This confirmed the modulus gradient of GPIL. The reasons for the gradient modulus and compressive strength of GPIL can be explained as follows. As it was presented in the FESEM images (**Figure 2b**), the higher monomer concentration resulted in the denser network with the thicker pore walls, which led to the higher compressive strength and Young's modulus of the PIL ionogel. The modulus of GPIL was 9 kPa, which was higher than that of PIL-1 but much lower than those of PIL-2 and PIL-3. The compressive stresses of GPIL at 80% and 81.5% strains reached 809 kPa and 1 MPa, respectively, slightly lower than that of PIL-3, but much higher than those of PIL-1 and PIL-2. GPIL and each layer of GPIL were able to recover after compression tests with the high pressure of 1 MPa, indicating the high elasticity of the ionogels (**Figure 3c, e** and **Figure S5**).

Stress-strain curves of GPIL (**Figure S4**) at different strain rates have also been measured. It was found that the stress-strain curve of the gradient PIL ionogel (GPIL) exhibited an apparent hysteresis loop, which became larger with higher strain rate, indicating a viscoelastic property. In addition, GPIL exhibited excellent fatigue resistance. It could recover its original size after compression tests with 50% strain for 100 cycles (**Figure 3f**). The multi-layer GPIL kept intact without inter-layer separation after cyclic compression tests. These characteristics of GPIL are necessary for a durable flexible pressure sensor.

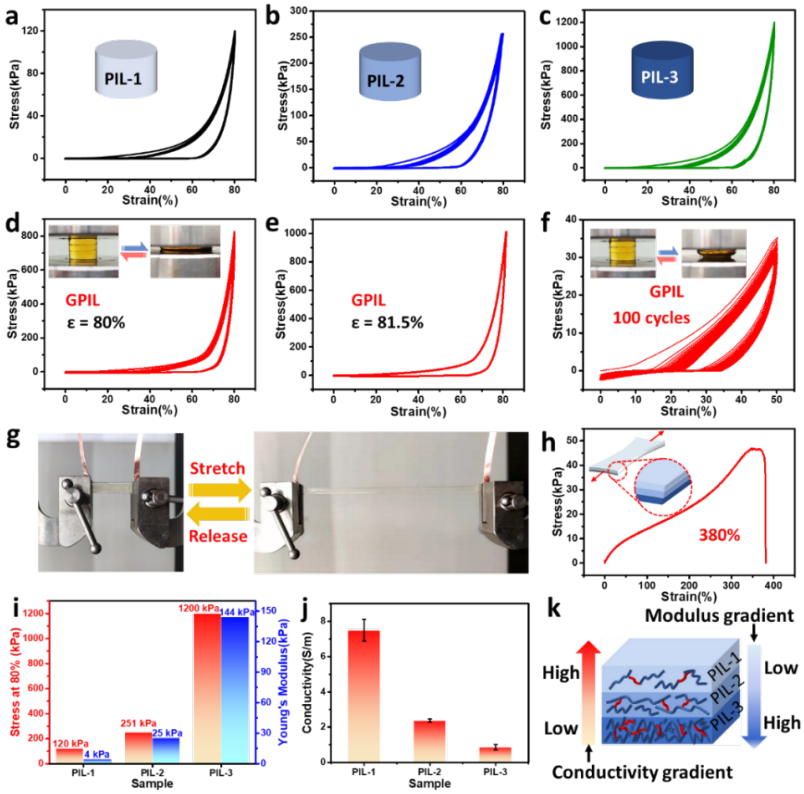

Figure 3. Mechanical properties of PIL iongels. Compressive stress-strain curves of (a) PIL-1, (b) PIL-2, (c) PIL-3, and (d, e, f) GPIL. (g, h) Tensile tests of GPIL. (i) Gradient Young's modulus and compressive stress (at 80% strain) of GPIL. (j) Gradient conductivity of GPIL. (k) Schematic of the modulus and conductivity gradient of GPIL.

In addition to high compressibility, GPIL exhibited high stretchability, which was confirmed by the tensile tests (**Figure 3g, h**, **Figure S6**, and **Movie S2**). The rectangular GPIL was cut into strips with a width of 8 mm and a thickness of 2.5 mm for the tensile tests. As shown in the tensile stress-strain curve of GPIL (**Figure 3h**), its elongation at break reached approximately 380%. As presented in the cyclic tensile test (**Figure S7**), GPIL could endure stretching with 320% strain for 4 cycles. The high compressibility, high stretchability, and high elasticity of GPIL were probably attributed to its tough three-dimensional network that was composed of flexible PIL polymers. These PIL polymers were chemically cross-linked by the cross-linker MBA during radical polymerization.

The electrical properties are also very important for flexible electronic devices. The abundant charged groups of ionic liquid could serve as free charge carriers, endowing the PIL ionogels with excellent electrical conductivities. In order to explore the effect of the monomer concentrations on the electrical properties of the PIL ionogels, we measured the electrical resistances of PIL-1, PIL-2, and PIL-3. PIL-1, PIL-2, and PIL-3 were kept in tight contact with each other at room temperature for 2 days to make sure that the diffusion of ions within the three ionogels reached equilibrium before resistance measurements. The conductivities (σ) were calculated by the following equation,

$$\sigma = \frac{L}{R \times S} \quad (1)$$

where R is the electrical resistance, L and S are the length and cross section area of the PIL ionogels, respectively. Based on the calculation results, the conductivity distribution of GPIL was depicted in **Figure 3j**. The conductivities of PIL ionogels decreased with increasing the monomer concentrations, the values of which were 7.5 S m^{-1}, 2.5 S m^{-1}, and 0.8 S m^{-1} for PIL-1, PIL-2, and PIL-3, respectively.

The mobility of ions plays a decisive role in the electrical conductivities of PIL ionogels. The higher monomer concentration resulted in a denser network, which would restrict the migration of free ions. Meanwhile, the denser network of the PIL ionogel would result in less mobile charge carriers even after the diffusion of ions reached equilibrium. These two factors led to the decrease of the conductivities of PIL ionogels with increasing the monomer concentrations.

It can be found that both the mechanical properties and electrical properties (electrical conductivity) of the PIL ionogels could be effectively adjusted by changing the monomer concentrations. Consequently, the modulus/conductivity-dual-gradient PIL ionogel can be obtained by superimposing three layers of ionogels with different monomer concentrations via the layer-by-layer gelation method (**Figure 3k**).

Gels with ionic conductivities and excellent flexibility have received lots of attention and are thought to be ideal candidates for wearable electronics. However, there are still plenty of inherent limitations of soft ionogels in achieving broader detecting range. In this work, a multi-layer gradient PIL ionogel was designed and used to assemble the resistive pressure sensor, which was expected to achieve the goal of wider-range pressure sensing. As shown in **Figure 4a**, the multi-layer GPIL was sandwiched between two flexible electrodes to afford a pressure sensor. Similarly, the electrical signals of the homogeneous PIL ionogel-based sensors were measured under different pressures for comparison. **Figure 4b** and **Figure S8** plotted the relative conductance changes ($\Delta G/G_0$) of the pressure sensors based on homogeneous

PIL ionogels and GPIL as a function of pressure. It was shown that the upper pressure detection limits of the sensors based on PIL-1, PIL-2, and PIL-3 were 120 kPa, 251 kPa, and 1200 kPa, respectively. By comparing the upper detection limits, it could be easily found that the sensors based on the PIL ionogels with higher compressive strengths had the higher upper detection limits. The upper detection limit of the GPIL-based sensor reached 1 MPa, which was slightly lower than that of the PIL-3-based sensor, but much higher than those of the sensors based on PIL-1 and PIL-2.

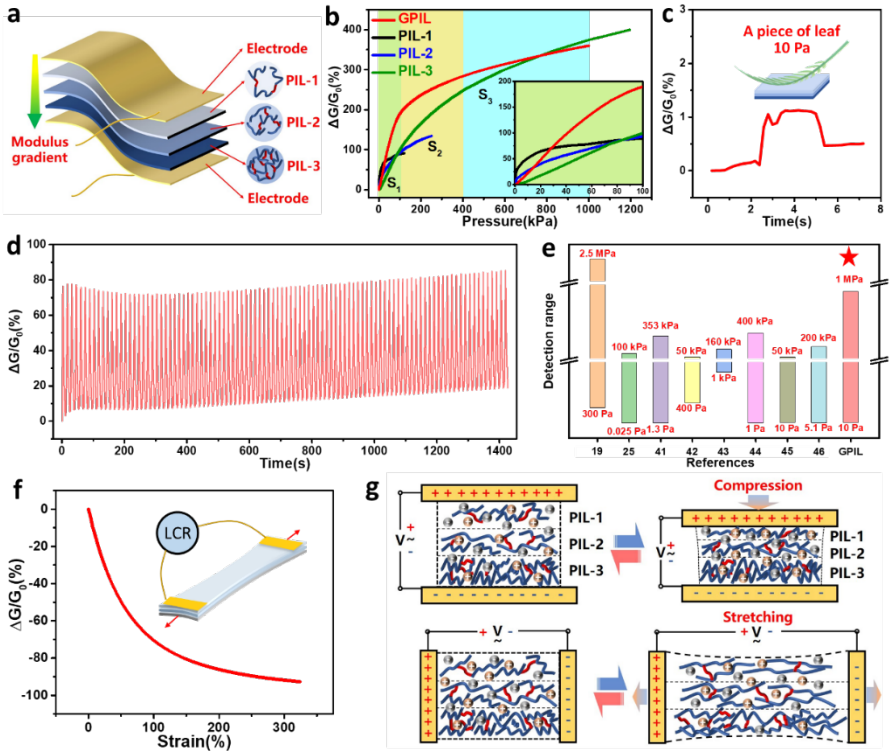

Figure 4. Sensing properties and mechanisms of the GPIL-based pressure sensor. (a) Schematic of the GPIL-based pressure sensor. (b) Relative conductance changes of the pressure sensors based on GPIL, PIL-1, PIL-2, and PIL-3 as a function of pressure (the inset is the partial-enlarged view in the range of 0-100 kPa). (c) Detection limit of the GPIL-based pressure sensor. (d) Loading-unloading cyclic test of the GPIL-based pressure sensor for 100 cycles with 50% compressive strain. (e) Comparison of the pressure detection ranges of our gradient PIL ionogel-based pressure sensor and other reported gel-based pressure sensors. (f) Relative conductance change of the GPIL-based sensor as a function of tensile strain. (g) Schematic of molecular-scaled structure variation of the GPIL-based pressure/strain sensor during compression and stretching.

The sensitivity, defined as the slope of the relative conductance change versus pressure, is a crucial parameter for wearable pressure sensors. As shown in **Figure 4b** and **Figure S8**, all of the sensors had relatively high sensitivities in their low-pressure range, and showed decreased sensitivities in their high-pressure range. In the low-pressure range (<10 kPa), PIL-1-based sensor had the highest sensitivity (0.04 kPa^{-1} within 0.5-10 kPa) while PIL-3-based sensor had the lowest sensitivity (0.0065 kPa^{-1} within 0.5-10 kPa). This can be explained that the PIL ionogels with lower moduli are softer and will have a more significant electrical signal change under the same external pressure, which is conducive to achieve a higher sensitivity in the low-pressure range.

The pressure sensitivity of the GPIL-based sensor was around 0.020 kPa^{-1}, 0.003 kPa^{-1}, and 0.002 kPa^{-1} in the range of 0-100 kPa, 100-400 kPa, and 400-1000 kPa, respectively. In the range of 0-100 kPa, the GPIL-based pressure sensor showed higher sensitivity compared with that of the PIL-3-based pressure sensor. In the range of 100-400 kPa, the relative conductance changes of the pressure sensors based on PIL-1 and PIL-2 tended to become saturated, while the pressure sensors based on GPIL and PIL-3 still exhibited relatively high sensitivities. In the range of 400-1000 kPa, the relative conductance changes of the pressure sensors based on GPIL and PIL-3 remained increasing with increasing pressure. This phenomenon can be explained as follows. When the GPIL-based pressure sensor is subjected to external pressures, the low-modulus layer first bears most of the deformation, resulting in the rapid increase of conductivity. Then, the compression deformation gradually shifts to the high-modulus layer when the softer layer approaches the saturation, alleviating the trend of saturation of the conductivity variation and ensuring the continuous change of the electrical signal. The low-modulus ionogel layer enabled the GPIL-based pressure sensor to exhibit excellent response to tiny pressures and strains, while the high-modulus layer ensured its response to high pressures.

As presented in **Figure 4c**, the measured detection limit of the GPIL-based pressure sensor was as low as 10 Pa. Combining the low-modulus layers and the high-modulus layers, the multi-layer gradient PIL ionogel-based sensor could detect wide-range pressures from 10 Pa to 1 MPa. In addition, the stability of GPIL-based pressure sensor was evaluated by loading-unloading cyclic test for 100 cycles with 50% compressive strain (**Figure 4d**). It can be seen that the sensor transformed the repeated deformations into stable electrical signal outputs. Benefitting from its wide pressure detection

range, the pressure sensor based on the gradient PIL ionogel is expected to achieve accurate measurement of tiny pressures as well as high pressures.

Figure 4e showed the comparison of the pressure detection ranges of our gradient PIL ionogel-based pressure sensor and other reported gel-based pressure sensors. The GPIL-based pressure sensor had an obvious advantage of wide detection range (10 Pa-1 MPa) over the reported gel-based pressure sensors.[19, 25, 41-46]

Apart from the compressive pressure sensing, the tensile strain sensing performances of the gradient PIL ionogel-based sensor were also examined. As shown in **Figure 4f** and **Figure S9**, the conductivity of GPIL-based strain sensor decreased with increasing tensile strain (in the range of 0-320%) or tensile stress (in the range of 0-40 kPa), and then gradually raised during unloading process, indicating a good tensile strain sensing performance.

The molecular-scaled structure variation during compression and stretching was schematically presented in **Figure 4g**. The conductance was markedly influenced by the migration of ions through the ionogel from one electrode to another electrode under an alternating voltage. During compression, the relative concentration of ions in the ionogel increased with shortened migration distances in a definite space, resulting in the increase of conductance.[19] There was an opposite situation during stretching, causing the decrease of conductance. Moreover, when the ionogel was released from compression or stretching, its conductance could recover its original value.

For the purpose of understanding the deformations of homogenous PIL ionogels and gradient PIL ionogel under various stresses more clearly, a simulation diagram was displayed in **Figure 5**. The strains of PIL-1, PIL-2, and PIL-3 under different stresses were assigned according to the stress-strain data obtained from **Figure 3a-c** and **Figure S5**. The strains of GPIL under different stresses listed in this diagram were theoretical values, which were calculated from the strains of PIL-1, PIL-2, and PIL-3 via the following equation,

$$\varepsilon = \frac{1}{3}(\varepsilon_1 + \varepsilon_2 + \varepsilon_3) \quad (2)$$

where ε is the theoretical strain values of GPIL, ε_1, ε_2, and ε_3 are the strain values of PIL-1, PIL-2, and PIL-3 under the same stress, respectively. The theoretical strains of GPIL at different stresses were basically consistent with the experimental strains obtained from the stress-strain curve of GPIL (**Figure S10**). **Equation 2** was used under the condition that each layer possessed the same thickness. However, the thicknesses of these three ionogel layers of the obtained GPIL may be slightly different, which resulted in the slight differences between the measured and calculated strains at the same pressure. Different levels of pressures including 1 kPa, 10 kPa, 100 kPa, and 1000 kPa were marked out in the diagram, and the deformations of the PIL ionogels under wide-range pressures could be intuitively observed. The softer PIL ionogel layer with a lower modulus exhibited a larger deformation under the same pressure compared with the stiffer PIL ionogel with a higher modulus. GPIL always showed a larger deformation compared to that of PIL-3 under the same pressure in the wide range of 0-1 MPa. Besides, the deformations of PIL-1 and PIL-2 became saturated under 1 MPa. By contrast, GPIL was compressible even under the high pressure of 1 MPa mainly due to the deformation of the layer with the highest modulus (PIL-3), indicating its feasibility for high-pressure sensing.

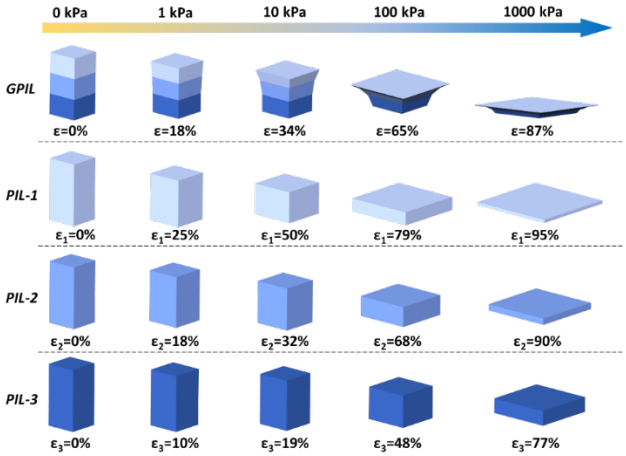

Figure 5. Simulation diagram of GPIL and corresponding homogenous ionogels (PIL-1, PIL-2, and PIL-3) under various stresses.

Thanks to the design of multi-layer gradient structure, the GPIL-based pressure sensor could detect wide-range pressures with high sensitivities. In addition, the PIL ionogels themselves have many advantages such as inherent excellent ionic conductivity, high tensile strength, high optical transparency, and high environmental stability. The gradient structure, ionic conductivity, flexibility, upper detection limit, and self-healing property of the resultant gradient PIL ionogel-based flexible pressure sensor are similar to those of the human skin. The high-performance wide-range pressure sensor based on GPIL can be used to monitor various physiological signals and human bodily motions and can also be applied for bioinspired ionic skins with a wide pressure response range.

The GPIL-based pressure/strain sensor was placed on different positions of human skins with the softest layer inside for the sensing demonstrations. The movements of the human body were recorded in real time by the sensor. Here, the changes of relative resistance and conductance were taken as the sensing parameters, which were calculated via the following formulas,

$$\frac{\Delta R}{R_0} = \frac{R - R_0}{R_0} \times 100\% \quad (3)$$

$$\frac{\Delta G}{G_0} = \frac{G - G_0}{G_0} \times 100\% \quad (4)$$

where R and G are the resistance and conductance values in real time, respectively, R_0 and G_0 are the initial resistance and conductance of the PIL ionogel, respectively.

Tiny pressures or strains could be detected by the GPIL-based pressure/strain sensor owing to its high sensitivity. By attaching the sensor to the skin of a volunteer's larynx, different words spoken by the volunteer could be distinguished and the swallowing actions could be accurately monitored (**Figure 6a, b**). The output signals of different words "Hi" and "Chinese" presented one peak and three peaks, respectively. Repeating each word twice could get the similar results, which proved the good discrimination and repeatability of the signal (**Figure 6a**). As shown in **Figure 6b**, the output signals were clearly recorded during swallowing.

The characteristics of each cycle of the output signals were similar during repeated swallowing for three times.

Figure 6c showed a real-time periodic pulse record detected by the GPIL-based pressure sensor attached on the volunteer's wrist. The heart rate (65 beats per minute) of the volunteer could be calculated from the peaks of the curve. There were three distinct peaks of P_1, P_2, and P_3 in the selected peak. P_1 was resulted from the blood flow ejected by heart contraction, while P_2 and P_3 were blood reflections from the lower body and closed aortic valve, respectively.[47] These results indicate the application potential of the GPIL-based pressure sensor in accurate personal health monitoring.

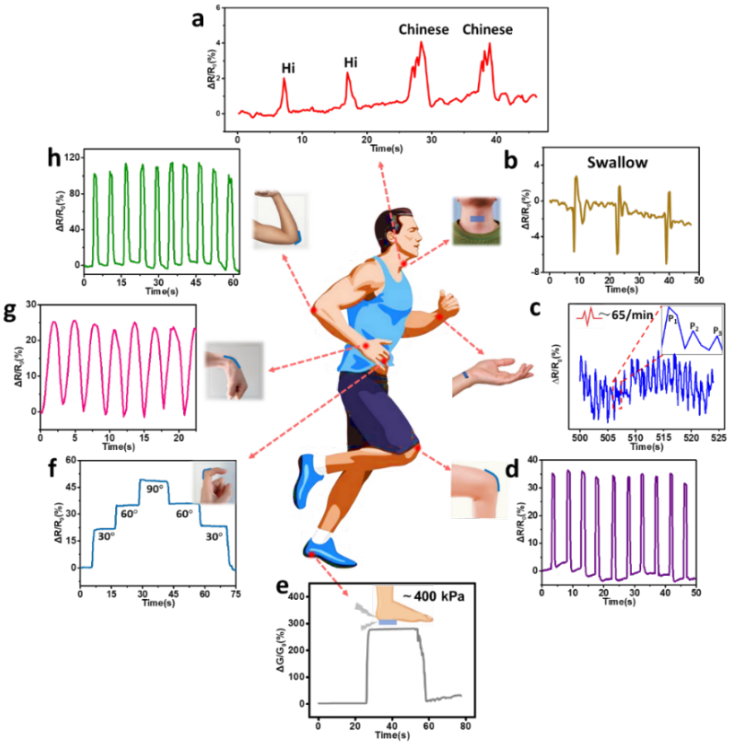

Figure 6. Detections of physiological signals and human bodily motions using the GPIL-based pressure/strain sensors. (a) Discrimination of different words. (b) Swallow monitoring. (c) Heart beat monitoring. (d) Movement detection of a knee. (e) Plantar pressure monitoring. (f) Finger bending monitoring. (g) Movement detection of a wrist. (h) Movement detection of an elbow.

In addition, it was found in **Figure 6f** that the relative resistance of the GPIL-based sensor increased with the increase of the finger bending angle. The relative resistance could recover its original value when the finger returned to the original angle, which showed the excellent repeatability of the signal. Similarly, when detecting the repeatedly bent and straightened movements of the wrist, elbow, and knee, the GPIL-based pressure sensor could output apparent electrical signals with good repeatability (**Figure 6d, g, h**). The recognition of motion states of human joints by the flexible sensor will help to realize the real-time and remote operations of robot motions in the future, which is expected to promote the development of human-computer interaction interface and artificial intelligence.

Further demonstrations were carried out to evaluate the application of the GPIL-based pressure sensor in wide-range pressure sensing. It is noteworthy that the upper pressure limit of the GPIL-based pressure sensor (1 MPa) is high enough to detect the plantar pressures of a person. The GPIL-based pressure sensor was put on the sole of the volunteer to monitor the plantar pressures. As shown in **Figure 6e**, when the body of a volunteer was supported with his feet, the relative conductance change of the GPIL-based pressure sensor reached around 280% immediately. After the foot was lifted, the relative conductance change decreased rapidly to the original value. The successful detection of the plantar pressure by the GPIL-based sensor validated its high potential for practical applications in wide-range pressure sensing.

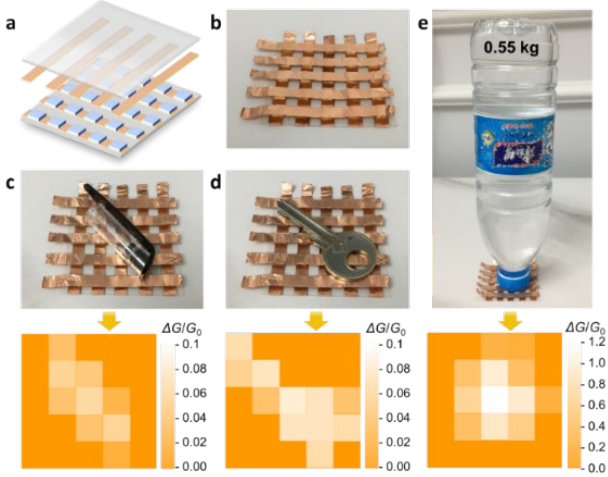

Figure 7. GPIL-based pressure-sensing array. (a) Schematic of the structure of the sensing array. (b) Photograph of the sensing array. Responses of the sensing array to (c) a cap of a pen, (d) a key, and (e) a bottle of water.

Besides, a high-performance 5×5 GPIL-based pressure-sensing array was demonstrated. The sensing array was mainly composed of 25 GPILs with the same size, 10 copper membrane strips, and two flexible and transparent insulators (**Figure 7a, b**). The signal outputs

of the sensing array were consisted with the positions and shapes of both the small and light-weight subjects (such as a cap of a pen and a key) and relatively large and heavy subjects (such as a bottle of water (0.55 kg)) that put on the array (**Figure 7c-e**). This also confirms the capability of the gradient PIL ionogel-based pressure sensor for wide-range pressure sensing.

In summary, we have developed a flexible pressure sensor with an ultrabroad detection range based on a novel gradient PIL ionogel, which was inspired by the gradient structure of the bamboo culms. The gradient PIL ionogel exhibited a unique modulus/conductivity-dual-gradient multi-layer structure, which was achieved by superimposing three layers of PIL ionogels with different monomer concentrations via the layer-by-layer gelation method. The modulus, compressive strength, and conductivity of the ionogel could be adjusted in a wide range by adjusting the monomer concentrations. The low-modulus ionogel layer enabled the gradient PIL ionogel-based pressure sensor to exhibit high response to tiny pressures and strains, while the high-modulus layer ensured its response to high pressures. As a result, the gradient ionogel-based pressure sensor showed a wide detection range of 10 Pa-1 MPa. It could be used for monitoring both tiny pressures (10-100 Pa) and high pressures (0.1-1 MPa) of various physiological signals and human bodily motions and showed potential applications in ionic skins with a wide response range. The ionic liquid endowed the ionogels with high stability in environments and excellent anti-freezing performances, which could further widen the application scope. This work provided a versatile method for the design of flexible materials with gradient structures, which is of great significance to the structural design of the next-generation flexible smart devices.

Supporting Information

Experimental section; synthesis of the cylindrical gradient ionogel; self-adhesive property of the gradient ionogel; compressive stress-strain curves of PIL-1, PIL-2, and PIL-3 with 50% strain; compressive stress-strain curves of GPIL at different strain rates; compressive stress-strain curves of PIL-1 with 95% strain and PIL-2 with 90% strain; stretchability and elasticity of the gradient ionogel; cyclic tensile test of GPIL with 320% strain; relative conductance changes of the pressure sensors based on different ionogels as a function of pressure with 50% strain; relative conductance change of the GPIL-based sensor as a function of tensile stress and time; Theoretical and experimental strains of GPIL under different stresses; Synthesis parameters of PIL-1, PIL-2, PIL-3, and GPIL. (DOCX)

High stretchability and elasticity of the gradient ionogel and the recombined gradient ionogel after being cut into two pieces. (MP4)

Corresponding Authors

Jia Huang - School of Materials Science and Engineering, Tongji University, Shanghai 201804, P.R. China. Email: huangjia@tongji.edu.cn.

Guoqing Zu - School of Materials Science and Engineering, Tongji University, Shanghai 201804, P.R. China. Email: guoqingzu@tongji.edu.cn.

Author Contributions

Xiaoyu Zhang and Sheng Zeng contributed equally to this work.

Notes

The authors declare no competing financial interest.

ACKNOWLEDGMENT

This work was supported by the National Natural Science Foundation of China (61822405, 62074111), the Science & Technology Foundation of Shanghai (19JC1412402, 20JC1415600), the Shanghai Social Development Science and Technology Project (20dz1201800), the Beijing National Laboratory for Molecular Sciences (BNLMS201904), Shuguang Program supported by Shanghai Education Development Foundation and Shanghai Municipal Education Commission (18SG20), and the Fundamental Research Funds for the Central Universities (22120220180).

REFERENCES

(1) Ling, Y.; An, T.; Yap, L. W.; Zhu, B.; Gong, S.; Cheng, W. Disruptive, Soft, Wearable Sensors. Adv. Mater. 2020, 32, 1904664.

(2) Chortos, A.; Liu, J.; Bao, Z. Pursuing Prosthetic Electronic Skin. Nat. Mater. 2016, 15, 937-950. DOI: 10.1038/nmat4671.

(3) Yang, C.; Suo, Z. Hydrogel Ionotronics. Nat. Rev. Mater. 2018, 3, 125-142.

(4) Zhao, F.; Shi, Y.; Pan, L.; Yu, G. Multifunctional Nanostructured Conductive Polymer Gels: Synthesis, Properties, and Applications. Acc. Chem. Res. 2017, 50, 1734-1743.

(5) Shi, X.; Fan, X.; Zhu, Y.; Liu, Y.; Wu, P.; Jiang, R.; Wu, B.; Wu, H.-A.; Zheng, H.; Wang, J.; et al. Pushing Detectability and Sensitivity for Subtle Force to New Limits with Shrinkable Nanochannel Structured Aerogel. Nat. Commun. 2022, 13, 1119-1119.

(6) Guo, H.; Tan, Y. J.; Chen, G.; Wang, Z.; Susanto, G. J.; See, H. H.; Yang, Z.; Lim, Z. W.; Yang, L.; Tee, B. C. K. Artificially Innervated Self-Healing Foams As Synthetic Piezo-Impedance Sensor Skins. Nat. Commun. 2020, 11, 5747.

(7) Wu, Y.; Liu, Y.; Zhou, Y.; Man, Q.; Hu, C.; Asghar, W.; Li, F.; Yu, Z.; Shang, J.; Liu, G.; et al. A Skin-Inspired Tactile Sensor for Smart Prosthetics. Sci. Robot. 2018, 3, No. eaat0429.

(8) Bai, N.; Wang, L.; Wang, Q.; Deng, J.; Wang, Y.; Lu, P.; Huang, J.; Li, G.; Zhang, Y.; Yang, J.; et al. Graded Intrafillable Architecture-Based Iontronic Pressure Sensor with Ultra-Broad-Range High Sensitivity. Nat. Commun. 2020, 11, 209.

(9) Duan, J.; Liang, X.; Guo, J.; Zhu, K.; Zhang, L. Ultra-Stretchable and Force-Sensitive Hydrogels Reinforced with Chitosan Microspheres Embedded in Polymer Networks. Adv. Mater. 2016, 28, 8037-8044.

(10) Ge, G.; Zhang, Y.; Shao, J.; Wang, W.; Si, W.; Huang, W.; Dong, X. Stretchable, Transparent, and Self-Patterned Hydrogel-Based Pressure Sensor for Human Motions Detection. Adv. Funct. Mater. 2018, 28, 1802576.

(11) Sun, J.-Y.; Keplinger, C.; Whitesides, G. M.; Suo, Z. Ionic Skin. Adv. Mater. 2014, 26, 7608-7614.

(12) Li, S.; Pan, H.; Wang, Y.; Sun, J. Polyelectrolyte Complex-Based Self-Healing, Fatigue-Resistant and Anti-Freezing Hydrogels As Highly Sensitive Ionic Skins. J. Mater. Chem. A 2020, 8, 3667-3675.

(13) Zhou, H.; Lai, J.; Zheng, B.; Jin, X.; Zhao, G.; Liu, H.; Chen, W.; Ma, A.; Li, X.; Wu, Y. From Glutinous-Rice-Inspired Adhesive Organohydrogels to Flexible Electronic Devices Toward Wearable Sensing, Power Supply, and Energy Storage. Adv. Funct. Mater. 2022, 32, 2108423.

(14) Wei, Y.; Xiang, L.; Zhu, P.; Qian, Y.; Zhao, B.; Chen, G. Multifunctional Organohydrogel-Based Ionic Skin for Capacitance and Temperature Sensing toward Intelligent Skin-Like Devices. Chem. Mater. 2021, 33, 8623-8634.

(15) Su, G.; Zhang, Y.; Zhang, X.; Feng, J.; Cao, J.; Zhang, X.; Zhou, T. Soft yet Tough: A Mechanically and Functionally Tissue-Like Organohydrogel for Sensitive Soft Electronics. Chem. Mater. 2022, 34, 1392-1402.

(16) Zhang, Z.; Wang, L.; Yu, H.; Zhang, F.; Tang, L.; Feng, Y.; Feng, W. Highly Transparent, Self-Healable, and Adhesive Organogels for Bio-Inspired Intelligent Ionic Skins. ACS Appl. Mater. Interfaces 2020, 12, 15657-15666.

(17) Liu, Y.-F.; Liu, Q.; Long, J.-F.; Yi, F.-L.; Li, Y.-Q.; Lei, X.-H.; Huang, P.; Du, B.; Hu, N.; Fu, S.-Y. Bioinspired Color-Changeable Organogel Tactile Sensor with Excellent Overall Performance. ACS Appl. Mater. Interfaces 2020, 12, 49866-49875.
(18) Yiming, B.; Guo, X.; Ali, N.; Zhang, N.; Zhang, X.; Han, Z.; Lu, Y.; Wu, Z.; Fan, X.; Jia, Z.; et al. Ambiently and Mechanically Stable Ionogels for Soft Ionotronics. Adv. Funct. Mater. 2021, 31, 2102773.
(19) Ren, Y.; Liu, Z.; Jin, G.; Yang, M.; Shao, Y.; Li, W.; Wu, Y.; Liu, L.; Yan, F. Electric-Field-Induced Gradient Ionogels for Highly Sensitive, Broad-Range-Response, and Freeze/Heat-Resistant Ionic Fingers. Adv. Mater. 2021, 33, No. e2008486.
(20) Gao, L.; Wang, M.; Wang, W.; Xu, H.; Wang, Y.; Zhao, H.; Cao, K.; Xu, D.; Li, L. Highly Sensitive Pseudocapacitive Iontronic Pressure Sensor with Broad Sensing Range. Nano-Micro Lett. 2021, 13, 140.
(21) Yang, P.; Shi, Y.; Li, S.; Tao, X.; Liu, Z.; Wang, X.; Wang, Z. L.; Chen, X. Monitoring the Degree of Comfort of Shoes In-Motion Using Triboelectric Pressure Sensors with an Ultrawide Detection Range. ACS Nano 2022, 16, 4654-4665.
(22) Ye, Y.; Zhang, Y.; Chen, Y.; Han, X.; Jiang, F. Cellulose Nanofibrils Enhanced, Strong, Stretchable, Freezing-Tolerant Ionic Conductive Organohydrogel for Multi-Functional Sensors. Adv. Funct. Mater. 2020, 30, 2003430.
(23) Lu, P.; Wang, L.; Zhu, P.; Huang, J.; Wang, Y.; Bai, N.; Wang, Y.; Li, G.; Yang, J.; Xie, K.; et al. Iontronic Pressure Sensor with High Sensitivity and Linear Response over a Wide Pressure Range Based on Soft Micropillared Electrodes. Sci. Bull. 2021, 66, 1091-1100.
(24) Liu, H.; Wang, X.; Cao, Y.; Yang, Y.; Yang, Y.; Gao, Y.; Ma, Z.; Wang, J.; Wang, W.; Wu, D. Freezing-Tolerant, Highly Sensitive Strain and Pressure Sensors Assembled from Ionic Conductive Hydrogels with Dynamic Cross-Links. ACS Appl. Mater. Interfaces 2020, 12, 25334-25344.
(25) Lee, Y.; Myoung, J.; Cho, S.; Park, J.; Kim, J.; Lee, H.; Lee, Y.; Lee, S.; Baig, C.; Ko, H. Bioinspired Gradient Conductivity and Stiffness for Ultrasensitive Electronic Skins. ACS Nano 2021, 15, 1795-1804.
(26) Song, S.; Zhang, C.; Li, W.; Wang, J.; Rao, P.; Wang, J.; Li, T.; Zhang, Y. Bioinspired Engineering of Gradient and Hierarchical Architecture into Pressure Sensors toward High Sensitivity within Ultra-Broad Working Range. Nano Energy 2022, 100, 107513.
(27) Zeng, S.; Zhang, J.; Zu, G.; Huang, J. Transparent, Flexible, and Multifunctional Starch-Based Double-Network Hydrogels As High-Performance Wearable Electronics. Carbohydr. Polym. 2021, 267, 118198.
(28) Zhang, S.; Zhou, Z.; Zhong, J.; Shi, Z.; Mao, Y.; Tao, T. H. Body-Integrated, Enzyme-Triggered Degradable, Silk-Based Mechanical Sensors for Customized Health/Fitness Monitoring and in Situ Treatment. Adv. Sci. 2020, 7, 1903802.
(29) Xiang, S.; Zheng, F.; Chen, S.; Lu, Q. Self-Healable, Recyclable, and Ultrastrong Adhesive Ionogel for Multifunctional Strain Sensor. ACS Appl. Mater. Interfaces 2021, 13, 20653-20661.
(30) Shahzadi, K.; Xiong, W.; Shekh, M.; Stadler, F. J.; Yan, Z.-C. Fabrication of Highly Robust and Conductive Ion Gels Based on the Combined Strategies of Double-Network, Composite, and High-Functionality Cross-Linkers. ACS Appl. Mater. Interfaces 2020, 12, 49050-49060.
(31) Singh, S. K.; Savoy, A. W. Ionic Liquids Synthesis and Applications: An Overview. J. Mol. Liq. 2020, 297, 112038.
(32) Nordness, O.; Brennecke, J. F. Ion Dissociation in Ionic Liquids and Ionic Liquid Solutions. Chem. Rev. 2020, 120, 12873-12902.
(33) Peng, X.; Liu, H.; Yin, Q.; Wu, J.; Chen, P.; Zhang, G.; Liu, G.; Wu, C.; Xie, Y. A Zwitterionic Gel Electrolyte for Efficient Solid-State Supercapacitors. Nat. Commun. 2016, 7, 11782.
(34) Wang, X.; Zhu, H.; Girard, G. M. A.; Yunis, R.; MacFarlane, D. R.; Mecerreyes, D.; Bhattacharyya, A. J.; Howlett, P. C.; Forsyth, M. Preparation and Characterization of Gel Polymer Electrolytes Using Poly(Ionic Liquids) and High Lithium Salt Concentration Ionic Liquids. J. Mater. Chem. A 2017, 5, 23844-23852.
(35) Zhang, S.-Y.; Zhuang, Q.; Zhang, M.; Wang, H.; Gao, Z.; Sun, J.-K.; Yuan, J. Poly(Ionic Liquid) Composites. Chem. Soc. Rev. 2020, 49, 1726-1755.
(36) Liu, Z.; Wang, Y.; Ren, Y.; Jin, G.; Zhang, C.; Chen, W.; Yan, F. Poly(Ionic Liquid) Hydrogel-Based Anti-Freezing Ionic Skin for a Soft Robotic Gripper. Mater. Horiz. 2020, 7, 919-927.
(37) Silva, E. C. N.; Walters, M. C.; Paulino, G. H. Modeling Bamboo as a Functionally Graded Material: Lessons for the Analysis of Affordable Materials. J. Mater. Sci. 2006, 41, 6991-7004.
(38) Yao, S.; Shen, J.; Guo, Y.; Zuo, S.; Shi, F.; Jiang, J.; Chu, J. Poly(Vinyl Alcohol)/Phosphoric Acid Gel Electrolyte@Polydimethylsiloxane Sponge for Piezoresistive Pressure Sensors. J. Mater. Chem. B 2021, 9, 8676-8685.
(39) Feng, S.; Li, Q.; Wang, S.; Wang, B.; Hou, Y.; Zhang, T. Tunable Dual Temperature-Pressure Sensing and Parameter Self-Separating Based on Ionic Hydrogel via Multisynergistic Network Design. ACS Appl. Mater. Interfaces 2019, 11, 21049-21057.
(40) Sun, J.-Y.; Zhao, X.; Illeperuma, W. R. K.; Chaudhuri, O.; Oh, K. H.; Mooney, D. J.; Vlassak, J. J.; Suo, Z. Highly Stretchable and Tough Hydrogels. Nature 2012, 489, 133-136.
(41) Lee, Y.; Park, J.; Cho, S.; Shin, Y.-E.; Lee, H.; Kim, J.; Myoung, J.; Cho, S.; Kang, S.; Baig, C.; et al. Flexible Ferroelectric Sensors with Ultrahigh Pressure Sensitivity and Linear Response over Exceptionally Broad Pressure Range. ACS Nano 2018, 12, 4045-4054.
(42) Cho, S. H.; Lee, S. W.; Yu, S.; Kim, H.; Chang, S.; Kang, D.; Hwang, I.; Kang, H. S.; Jeong, B.; Kim, E. H.; et al. Micropatterned Pyramidal Ionic Gels for Sensing Broad-Range Pressures with High Sensitivity. ACS Appl. Mater. Interfaces 2017, 9, 10128-10135.
(43) Qin, H.; Owyeung, R. E.; Sonkusale, S. R.; Panzer, M. J. Highly Stretchable and Nonvolatile Gelatin-Supported Deep Eutectic Solvent Gel Electrolyte-Based Ionic Skins for Strain and Pressure Sensing. J. Mater. Chem. C 2019, 7, 601-608.
(44) Zou, Q.; Ma, Z.; Li, S.; Lei, Z.; Su, Q. Tunable Ionic Pressure Sensor Based on 3D Printed Ordered Hierarchical Mesh Structure. Sens. Actuators, A 2020, 308, 112012.
(45) Jin, M. L.; Park, S.; Lee, Y.; Lee, J. H.; Chung, J.; Kim, J. S.; Kim, J.-S.; Kim, S. Y.; Jee, E.; Kim, D. W.; et al. An Ultrasensitive, Visco-Poroelastic Artificial Mechanotransducer Skin Inspired by Piezo2 Protein in Mammalian Merkel Cells. Adv. Mater. 2017, 29, 1605973.
(46) Li, S.; Chu, J.; Li, B.; Chang, Y.; Pan, T. Handwriting Iontronic Pressure Sensing Origami. ACS Appl. Mater. Interfaces 2019, 11, 46157-46164.
(47) Park, J.; Kim, M.; Lee, Y.; Lee, H. S.; Ko, H. Fingertip Skin-Inspired Microstructured Ferroelectric Skins Discriminate Static/Dynamic Pressure and Temperature Stimuli. Sci. Adv. 2015, 1, e1500661.